Multiple-panel Longwall Top Coal Caving Induced Microseismicity: Monitoring and Development of a Statistical Forecasting Model for Hazardous Microseismicity

Cao, W., Durucan, S., Cai, W., Shi, J.Q., Korre, A.

Department of Earth Science and Engineering, Royal School of Mines, Imperial College London, London, SW7 2AZ, United Kingdom

ABSTRACT: Continuous microseismic monitoring was carried out around 9 producing longwall top coal caving (LTCC) panels with concurrently recorded daily face advance rates at Coal Mine Velenje in Slovenia over a 27-month monitoring period. The monitoring results suggested that spatial and magnitude characteristics of microseismicity are dominated by those of underlying fractures, while microseismic event rate is under the combined effects of local natural fracture abundance and mining intensity. On this basis, a data-driven yet physics-based forecasting methodology was established for LTCC induced hazardous microseismicity, which is above a given threshold of energy magnitude and within a certain distance to the longwall face. Statistical analyses were first conducted to characterise temporal, magnitude and spatial characteristics of long-term recorded microseismicity, based on which a short-term forecasting model was developed to calculate the probability of hazardous microseismicity considering the three characteristics. The model developed was employed to forecast the likelihood of hazardous microseismicity at one of these LTCC panels, and the forecasted results were supported by the monitoring. This statistical model has important implications in the evaluation of mining-induced hazards, and it can be used to optimise longwall face advance rates to minimise the risk of hazardous microseismicity in burst-prone deep-level mining sites.

1. INTRODUCTION

As underground coal mining in Europe and worldwide extends to increasingly deep levels, it faces an increasing risk with respect to rockburst and coal and gas outburst hazards. Therefore early warning of rockbursts and gas outbursts is imperative to mine safety. Microseismic monitoring, as a potentially effective passive seismological monitoring tool, has been widely used to identify regions prone to seismic-induced hazards or give early warnings of the hazards.

The observation of anomalous increase in seismic activity prior to mining hazards, sometimes followed by returning to low levels, has been considered in earlier studies as a predictor of rock bursts (Brady, 1977), outbursts (Styles *et al*., 1988), and roof failure (Shen *et al*., 2008). Later on, extensive seismic risk assessment was performed through recognition of regularity patterns indicative of rockbursts, which are usually characterised by anomalous variations in microseismic precursors. Those microseismic precursors could be categorised as temporally-related (the number of large events, the ratio of the number of events of different energy, the variance of event counts at two

successive time moments, etc.), energy-related (sudden change of apparent volume, seismic stress drop, the deviation of seismicity from the long-term trend, *b* value, etc.), and spatially-related (fractal dimension, median distance between microseismic pairs, etc.) (Ma *et al*., 2018; Marcak, 1993; Stewart and Spottiswoode, 1993). However, each individual seismic index tends to identify different subsets of potentially-damaging events when applied in isolation, and the most effective seismic index may vary from site to site.

Since the 1990s, some comprehensive quantitative methods have been introduced to the forecasting of rockbursts and gas outbursts. The combination of seismological analysis and different methods, such as probabilistic methods (Lasocki, 1993), clustering analysis (Kijko *et al*., 1993), mathematical and physical modelling (Melnikov *et al*., 1996) and numerical stress analysis (Fujii *et al*., 1997), facilitates early risk assessment of mining hazards.

One common drawback of the current rock burst and gas outburst assessment and prevention methods referred to above is that their applications are mostly based on site-specific field experience, as opposed to sound physical

foundation. The success of the forecasting at a specific mine cannot necessarily guarantee the success in application to other rockburst-prone mining sites. In addition, mining activities are causes of microseismicity, but most forecasting methods focus only on the microseismic monitoring data itself, without incorporating the concurrent mining intensity. This can sometime lead to unreliable forecasting results, where the risk potential around a longwall face should obviously vary with scheduled mining intensity (ranging from complete cessation to full capacity operation), while the same risk potential would be estimated based solely on previous microseismic datasets.

In this work, microseismic data recorded around multiple longwall mining panels at Coal Mine Velenje is analysed, in conjunction with the prevailing face advances of the panels. It is recognised that microseismic characteristics are under the combined effects of attributes of fractures and mining intensity, which forms the basis for the development of a data-driven yet physics-based approach to mining hazard forecasting. The physical nature originates from characteristics of pre-existing natural fractures throughout the coal seam, which dominate the resulting microseismic patterns. In addition, mining intensity which plays a significant role in affecting event counts frequency is considered by coupling real time processing of the microseismic sequence data with mining exploitation schedule in this work. The physical base of the model allows to compare respective contributions of different influencing factors to the hazard potential, and to determine the dominant factor. To take a step further, the forecasting model could be used to regulate the face advance rate of longwall coal mining in real time.

2. IN SITU MICROSEISMIC MONITORING AT COAL MINE VELENJE

2.1. Coal Mine Velenje
Coal Mine Velenje is located in the north of Slovenia. The coal basin lies in a synclinal valley, which extends between the Šoštanj and Smrekovec faults. The mine currently mines a lens-shaped deposit, which extends to a length of 8.3 km in the WNW-ESE direction and has a width between 1.5 and 2.5 km (Fig. 1). The coal seam is 165 m thick in the central part and pinches out towards the margins. The Velenje Coal is a humic type lignite, the matrix of which is detrite-dominated, dark brownish to dusky brown in colour.
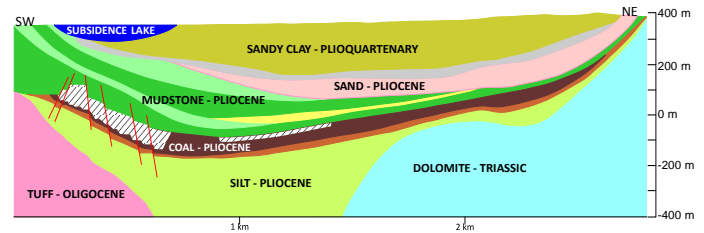

Fig. 1. Schematic SW–NE trending geological cross-section of the Velenje coalfield (after Markič and Sachsenhofer, 2010).

For efficient coal extraction from the ultra-thick coal seam, the multi-level longwall top coal caving (LTCC) method is practiced at the mine. Specifically, the entire coal deposit is divided into a number of levels ranging from 10 to 20 m in thickness, and extracted sequentially from the top to the bottom. At each level, the lower section of the seam (3-4 m in thickness) is cut by a shearer under the hydraulic supports, and the top coal (7-17 m in thickness) is allowed to cave by gravity and be recovered in front of the supports (Jeromel et al., 2010; Si et al., 2015).

Over one hundred years of coal production in the mine has resulted in a highly stressed central coal pillar, which is protecting the main infrastructure in the production districts, and is surrounded by multiple longwall panels (Fig. 2). Longwall coal production started at -80 m depth in 2015, and gradually transferred below to -95 m depth from 2017. Nine longwall panels have been in production sequentially during 2016-2019. Five panels, i.e. K.-80/B, K.-80/C, K.-80/D, K.-80/E, and CD2, are at -80 m level, with the other four (K.-95/A, K.-95/D, K.-95/E and CD3G) at -95 m level. Until today, panels K.-80/B, K.-80/C, K.-80/D, K.-80/E, K.-95/A and K.-95/E advanced in the southwest direction towards the central coal pillar, while CD2 and CD3G advanced at an angle of about 120° to the other panels away from the coal pillar.

To achieve full operation capacity with the mine staff and facilities, there were two longwall panels working concurrently over most of the production period. The two working panels were usually chosen separated spatially to spread out stress concentration around mined-out areas.

2.2. In Situ Microseismic Monitoring
The underground microseismic monitoring at Coal Mine Velenje was jointly conducted by Laboratory of Mining Geophysics of Central Mining Institute (GIG) in Poland and the mine staff. A 32-channel flameproof automated seismic observation system (SOS) developed in GIG was used for the underground microseismic monitoring.
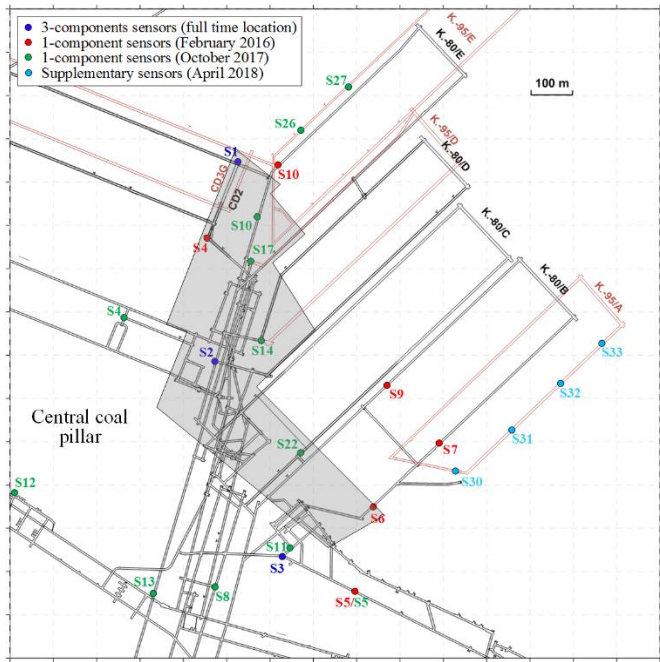
Fig. 2. Mine production layout during 2016-2018 at Coal Mine Velenje and distribution of installed seismic stations of the microseismic monitoring system.

The installed microseismic monitoring system at Coal Mine Velenje encompassed the nine LTCC panels in production around the central coal pillar. The SOS system consisting of 3 triaxial seismic sensors and 7 uniaxial seismic sensors was initially installed in the area of active longwall panels K.-80/B and K.-80/E at the beginning of seismic monitoring in February 2016. With the coal face movement, as well as to accommodate larger longwall coal mining-disturbed areas, later on the number of uniaxial seismic sensors was increased to 9 (from August 2016) and then 12 (from October 2017) (Fig. 2).

The recorded raw data were post-processed to identify microseismic events and obtain source parameters and event locations. First arrival and end times of seismic P and S waves needed to be determined for each seismic station (channel) and for each recorded seismic event to obtain location and seismic energy for each seismic event. As these parameters directly affect accuracy of seismic event location and seismic energy calculation, those times were picked manually in order to obtain maximum possible accuracy. The energy radiated from each microseismic event was calculated on the basis of time-integrated values of particle vibration velocities of P and S waves, respectively (Shearer, 1975).

2.3. Analysis of Field Recorded Microseismicity

During the monitoring period between 29 February 2016 and 20 May 2018, a total of over 17,000 microseismic events were identified around the eight LTCC panels at different levels. The complete record of the daily face advance at each LTCC panel was available, which allowed the recorded microseismicity to be correlated with the prevailing face-line positions.

To facilitate analysis in this work, each microseismic event was to be associated with one of the nine panels, which is active and whose working face-line position is located closest to the event. Here a longwall panel is considered to remain active within 7 days after the coal production is completed. It has been recognised that it usually takes a period of time for the stress field disturbed by longwall mining to reach a new state of equilibrium (Styles et al., 1988). Indeed, a few microseismic events were recorded at weekends when there was no active mining.

Microseismic events around a representative LTCC panel K.-80/B are analysed below. Fig. 3 presents the mined-out area and distribution of the associated microseismic events for the panel K.-80/B. The majority of microseismicity located within and close to the mined area. It is further noted that there was a kidney-shaped area where the density of the seismic events was relatively higher, indicating elevated stress concentration. A large part of this area is seen to overlap with the central coal pillar after the longwall panels were mined out. However, it is noteworthy that regions with dense microseismicity and intensive seismic energy release around the panel are not fully overlapped with the mined-out or stress concentrated areas, which strongly suggests that spatial and magnitude characteristics of the LTCC mining-induced microseismicity are to a large extent dominated by the attributes of underlying fractures.
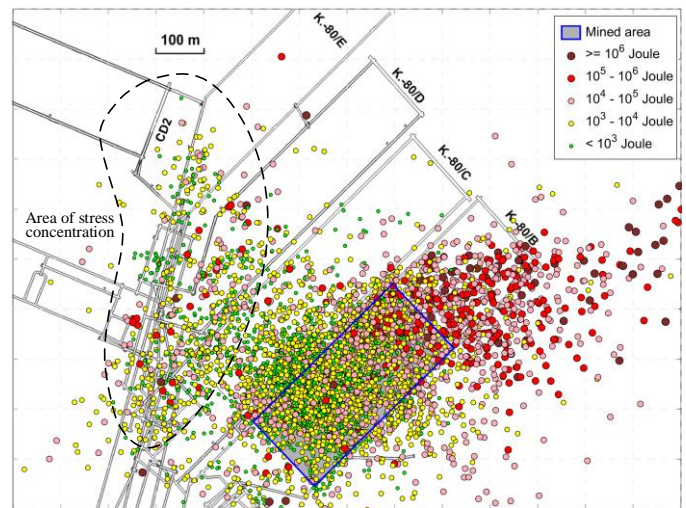

Fig. 3. Spatial distribution of microseismicity associated with panel K.-80/B.

Fig. 4 plots the daily event number, seismic energy released and the distance to the closest face-line, together with the daily face advance rate at panel K.-80/B. The distance to the closest face-line position is taken as the distance of microseismicity to the nearest point of the closest active longwall face. The results show that the daily microseismic intensity (top panel) closely follows the mine production schedule (bottom panel), with

reduced values at weekends and holidays. In contrast, the average seismic energy and distance to the nearest face-line remained relatively consistent throughout, with the exception of a few outliers existing due to the scarcity of event numbers at weekends. The latter suggests that the face advance rate had much less impact on the magnitude and spatial distribution of microseismicity.
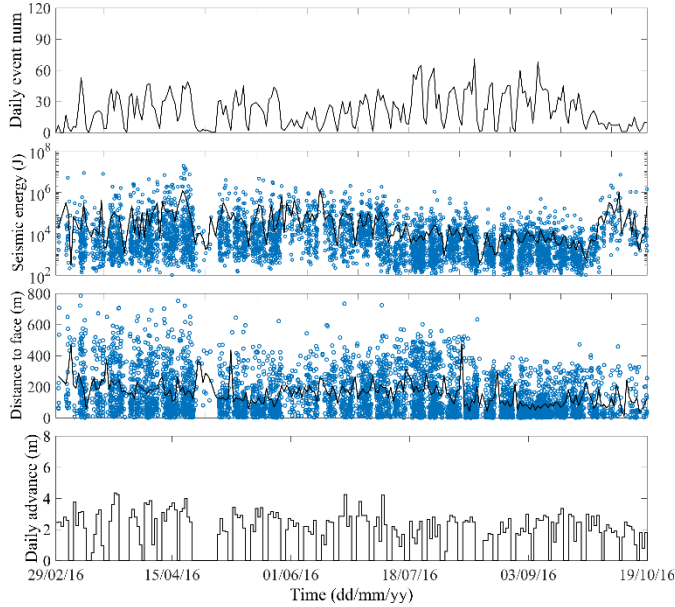

Fig. 4. Evolutional characteristics of LTCC mining-induced microseismicity on a daily basis around panel K.-80/B.

In an effort to minimise deviations caused by the insufficient number of events, analyses of seismic energy, in terms of the estimation of b value in the Gutenberg-Richter law and the box-and-whisker diagrams, were performed based on weekly events. To yield a reliable b value, which represents the scaling of seismic energy, the regression fitting was made over a linear part of the weekly frequency-magnitude plots, while discarding those weeks with few microseismic events.

A representative example of the results is presented in Fig. 5. The b values for the weekly microseismicity generally fluctuated around 1 (top panel). As the b value has an inverse correlation with the average seismic energy, the elevated level at panel K.-80/B during the period 17/07/16-02/10/16 indicates supressed seismic energy release, and vice versa when it subsequently dropped to the normal level.

It is noted that the face advance rate had little impacts on either the b value or the average seismic energy. In those weeks when coal extraction was halted in particular, both the b value and the average seismic energy remained fairly stable, albeit the number of newly generated microseismic events dropped significantly. This indicates that mine production as a trigger of microseismicity does not dominate the magnitude and scaling of the resulting energy release.
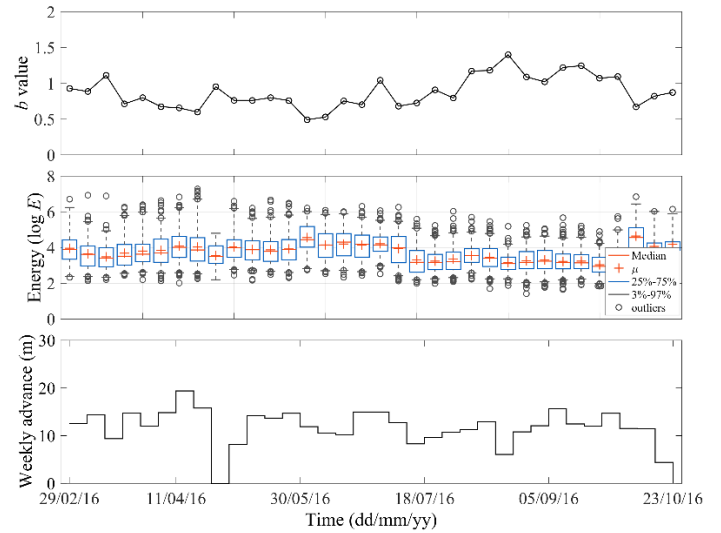

Fig. 5. Evolutional characteristics of LTCC mining-induced microseismicity on a weekly basis around panel K.-80/B.

3. A STATISTICAL MODEL TO FORECAST HAZARDOUS MICROSEISMICITY

The statistical forecasting model proposed in the present work is built based upon the understanding that mining-induced microseismicity is considered as slippage of fractures throughout the coal seam and surrounding rock strata triggered by mining excavation (Cao *et al.*, 2018). From the observations above, it was found that seismic energy magnitude and spatial distribution are dominated by those of underlying fractures (intrinsic factors), while microseismic event counts frequency is correlated with both local fracture abundance (intrinsic factor) and mining intensity (extrinsic factor). When extrinsic factors are reduced or eliminated by maintaining a constant mining intensity, recorded microseismicity, or the fractures that have already slipped as a subset of neighbouring fractures, reflect the spatial, temporal and magnitude characteristics of the neighbouring fracture field.

Discrete natural fractures are heterogeneously distributed throughout the coal seam and surrounding rock strata. Although discrete fractures are independent with each other, they are characterised by spatial continuity in terms of attributes, i.e., two regions close to each other are likely to have similar attributes (e.g., the density, size, scaling of nature fractures, etc.) than those that are far apart (Journel and Huijbregts, 1978). As such, the spatial continuity in geology would result in the segmental stationarity of microseismic characteristics, where statistical features of microseismicity happening close in time are relatively steady. On the other hand, anomalous variations in mining-induced microseismicity reflect variations in corresponding attributes of the fracture field, which are indicative of stress or geological heterogeneity and give pre-warnings for the increased hazard potential.

Microseismic events that are either of a large magnitude or with a short distance to working faces, are indicative of large potential of rockburst and gas outburst hazards in coal mines. In this work, hazardous microseismicity is defined as those having large energy release and happening close to working faces or roadways, which are the most threatening to mine workers and mining equipment. The real time forecasting of hazardous microseismicity, in this context, becomes the problem of estimating the time-varying possibility that at least a large fracture slips in the vicinity of coal extraction over a certain period, given the local fracture field and production schedule (Fig. 6). The statistical forecasting methodology presented in this work aims at resolving this problem by continuous evaluation of microseismic features representing characteristics of the local fracture field and mining intensity.
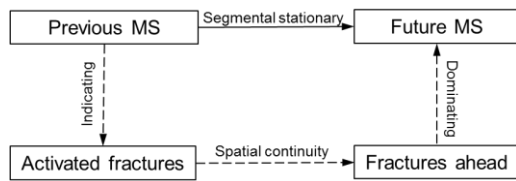

Fig. 6. Schematic diagram illustrating the physical basis of the statistical forecasting method for hazardous microseismicity.

As the first step for the risk assessment of rock bursts and gas outbursts, a sequence of longwall face advance and the associated microseismicity are recorded as inputs of the proposed methodology. Considering that geological conditions (fracture attributes in particular) and production schedule (represented by the face advance rate) are panel specific, the methodology is applied to microseismicity associated with longwall coal mining at each individual panel. The assessment of recorded sequence of microseismicity around a certain longwall panel involves filtering the most recent events using a moving time window of ΔT, assessing microseismic characteristics in a statistical manner, and using the fitted microseismic parameters as a basis for forecasting microseismicity that would occur over the next time interval Δt. This process is updated at the time interval Δt until the completion of the longwall panel. The procedure to forecast the potential of hazardous microseismicity at time t for the next time interval $[t, t+\Delta t]$ using microseismicity recorded in the time window $[t-\Delta T, t]$ involves the following steps.

The *fitting of distribution and parameter estimation* are first conducted for a suite of relevant characteristics such as event counts frequency, energy magnitude distribution and spatial distribution of mining-induced microseismicity within the time window. The statistical description of microseismic characteristics is described in Section 3.1.

Next, *estimation of probability of hazardous events* is performed based on the fitted statistical models of temporal, spatial and magnitude characteristics of microseismicity over the time window. The probability of hazardous events is regarded as the joint probability considering the aforementioned characteristics. In particular, the statistical forecasting model of event counts frequency incorporates the impact of the current face advance rate. The risk assessment of hazardous events is presented in Section 3.2.

In the final step, *computation of recommended upper limit of face advance* is carried out if the estimated probability exceeds a certain threshold. This is achieved by inversely calculating the face advance rate based on the proposed statistical model of joint probability. A flow chart of the forecasting methodology developed is presented in Fig. 7.
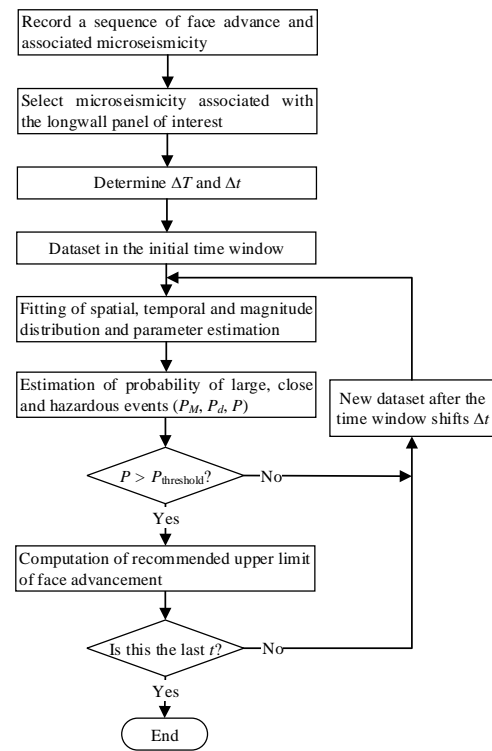

Fig. 7. Flow chart of the forecasting procedure using longwall mining-induced microseismic sequence datasets with concurrent face advance records around a longwall panel.

3.1. Statistical Characteristics of Microseismicity

(1) Event counts frequency
Event counts is defined as the number of microseismic events occurring over a time interval of Δt. Given a constant face advance rate, the generation of microseismicity can be approximately considered as a Poisson point process, which is described by the Poisson distribution. The probability distribution function (PDF) for n microseismic events taking place over a time interval of Δt from time t is a discrete probability distribution given by:

$$p(n) = \frac{[\lambda(t)\Delta t]^n e^{-\lambda(t)\Delta t}}{n!} \qquad (1)$$

where $\lambda(t)$ is the average event counts per unit time at time t. The evolution of $\lambda(t)$ reflects the varying abundance, or the local heterogeneity of fractures around the mining-disturbed region. Fig. 8 presents examples for the monitored and fitted event counts frequency of microseismicity around three longwall panels at Coal Mine Velenje. Due to the wide dispersion of the daily event counts, they are presented in groups with a bin interval of 10. It can be seen that the Poisson distribution gives a good fit to frequency of daily microseismic event counts around each panel.
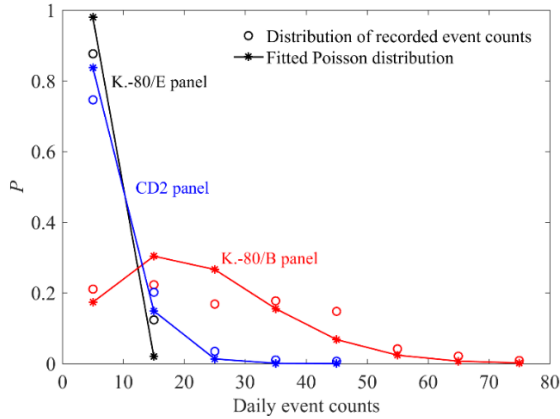

Fig. 8. Frequency of daily microseismic event counts associated with longwall coal mining at three longwall panels at the -80 m level at Coal Mine Velenje (the connecting lines are only guides for the eye).

Eq. (1) can be used to forecast the frequency of daily event counts to be induced under the same mining conditions (represented by the face advance rate). Since mining operation is a dynamic process, the ever-varying face advance rate should be accounted for in forecasting event counts. Based upon the analysis above, the face advance rate has a positive correlation with the number of recorded microseismicity, owing to the physical nature that the area of mining-disturbed region is linearly correlated with the number of slipped fractures for a relatively homogeneous fracture field. Therefore, a ratio η, defined as the face advance rate r during the next time interval over the average rate $\bar{r}$ during the previous monitoring period, should be used as a tuning coefficient in estimating the event counts frequency:

$$\eta = r / \bar{r} \qquad (2)$$

The modified PDF can be used to estimate the frequency of microseismic event counts over the next time interval Δt by fitting microseismic data within the time window of ΔT:

$$p(n) = \frac{[\eta\lambda(t)\Delta t]^n e^{-\eta\lambda(t)\Delta t}}{n!} \qquad (3)$$

The most probable seismic event count over the next time interval Δt is forecasted as $\eta\lambda(t)$.

(2) Energy magnitude distribution

As the previous work by the authors (Cao et al., 2018) suggests, the magnitude distribution of microseismic energy released is dominated by the size and scaling of slipped fractures. The frequency-magnitude distribution of microseismicity follows the empirical Gutenberg-Richter law (Richter, 1958). The Weibull distribution was found to achieve a better fit than the empirical (exponential) distribution of logarithmical seismic energy (Kijko et al., 1993; Lasocki, 1993). The CDF of the Weibull distribution is given by:

$$F(M) = 1 - \exp\left[-\left(\frac{M - M_{min}}{l_e(t)}\right)^{k_e(t)}\right] \quad (M \geq M_{min}) \qquad (4)$$

where M_{min} is the minimum energy magnitude in field microseismic monitoring, and $k_e(t)$ and $l_e(t)$ are shape and scale parameters at time t, respectively.

The CDF of the energy magnitude distribution can be fitted using microseismic data within the time window of ΔT to estimate the probability of a microseismic event with energy greater than a threshold over the next time interval Δt. Fig. 9 presents examples of the frequency-magnitude distribution and fitted Weibull distribution for field microseismic monitoring data at Coal Mine Velenje (the minimum detectable energy is 10^2 J so $M_{min} = 2$).
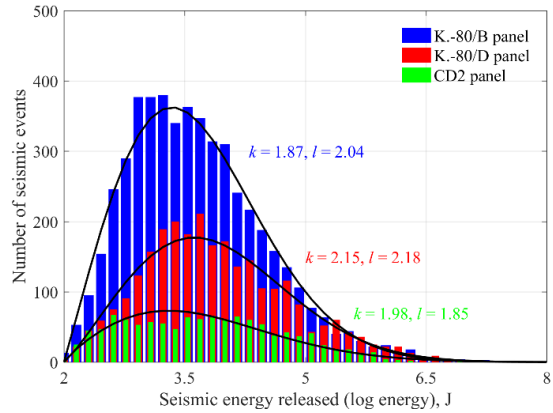

Fig. 9. Examples of recorded and fitted energy magnitude distribution for mining-induced microseismic events around different longwall panels at Coal Mine Velenje.

(3) Distance to the face-line position

The location of microseismicity reflects the spatial distribution of pre-existing nature fractures to a large extent. Given the same mining and stress conditions, the spatial clustering of microseismicity is attributed to the heterogeneous distribution of fractures. In this work, the distance of microseismicity to the face-line is introduced to represent the spatial distribution of underlying nature fractures. Spatial clustering of a group of microseismic

events can be characterised by a tall and thin histogram of distances to the face-line, while relatively homogeneous distribution of microseismicity yields a squat and fat histogram. Since microseismicity tends to cluster at fracture-intense regions, the average distance of microseismicity to the face-line dynamically changes with the advancing longwall face. A decrease in the average distance of microseismicity to the face-line suggests a higher chance of microseismicity occurring close to the longwall face as the mine production progresses, while an increase indicates the opposite.

Similar to the microseismic energy magnitude distribution, the spatial distribution of microseismicity with respect to the face-line is a continuous probability distribution and can be described by the Weibull distribution. The CDF is written as:

$$F(d) = 1 - \exp\left[-[d / l_d(t)]^{k_d(t)}\right] \tag{5}$$

where $k_d(t)$ and $l_d(t)$ are shape and scale parameters at time t, respectively.

The CDF of the spatial distribution of microseismicity with respect to the face-line can be fitted using microseismic data within the time window of ΔT to estimate the probability of a microseismic event falling within a certain distance to the face-line over the next time interval Δt. Fig. 10 presents examples of the spatial distribution with respect to the face-line and fitted Weibull distribution for field recorded microseismicity at Coal Mine Velenje. The distribution in the histograms for the three panels in Fig. 10 is skewed, with the peak located from 40 to 200 m with respect to the longwall face. The histograms suggest that microseismic events associated with coal mining at K.-80/B and K.-80/D panels are more spatially concentrated, while those at CD2 panel are much more scattered. The Weibull distribution is well-adapted to different histograms and fits the general trend well.
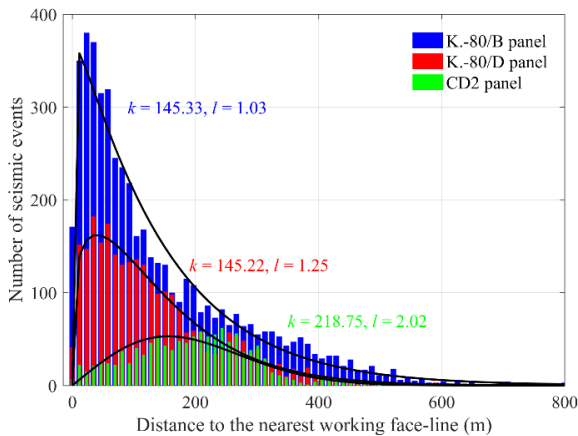

Fig. 10. Examples of recorded and fitted spatial distribution with respect to the face-line for microseismic events around different longwall panels at Coal Mine Velenje.

3.2. Risk assessment of hazardous events

From observations at Coal Mine Velenje, the spatial distribution of fractures, attributes of fractures, and mining activities can be considered as mutually independent. In particular, mining progression influences the area of extracted regions and in turn the number of slipped fractures per unit time, but not the size and scaling of fractures. Therefore, it is justified to estimate the probability of hazardous microseismicity as the joint probability of event occurrence, the probability of an event being a large event, and the probability of an event being close to the longwall face.

The probability that at least an event with a magnitude greater than M occurs in n microseismic events is written as:

$$p_M = 1 - F(M)^n \tag{6}$$

Considering the estimated event counts frequency from the Poisson distribution for field microseismic monitoring data over the most recent period ΔT, the probability that at least an event with a magnitude greater than M occurs over the next time interval Δt is:

$$P_M = \sum_n p(n)\left[1 - F(M)^n\right] \tag{7}$$

Likewise, the probability that at least an event with a distance less than d to the face-line occurs over the next time interval Δt is written as:

$$P_d = \sum_n p(n)\left[1 - (1 - F(d))^n\right] \tag{8}$$

In this work, a hazardous event is defined as a microseismic event with released energy greater than M and falling within a distance of d to the face-line. The probability of an individual seismic event being a hazardous event is the joint probability considering both the spatial and magnitude distributions:

$$p = [1 - F(M)]F(d) \tag{9}$$

The probability that at least a hazardous event occurs over the next time interval Δt is:

$$P = \sum_n p(n)\left[1 - (1 - p)^n\right] \tag{10}$$

Given a threshold for the probability of hazardous microseismicity, the inverse calculation of face advance can be achieved by combining Eqs. (3) and (10).

4. APPLICATION OF THE FORECASTING METHODOLOGY

The forecasting methodology developed was applied to recorded microseismicity associated with longwall coal mining at the panel K.-80/B, which was considered to have a complete record of mining-induced

microseismicity and consist of a relatively large number of events (>2,500 events each).

The length of time window ΔT needs to be determined based on the event rate and mining schedule. Segmental stationarity needs to be achieved for microseismicity within this interval to give a reliable estimation of parameters. In this sense, the interval should be sufficiently long to allow for mining-induced stress adjustment and re-equilibrium. As a reference, the time needed for microseismicity to fade out after mining completion or to achieve normal levels of seismicity after re-operation was around 1 week, according to the observations above and literatures (Styles *et al*., 1988). On the other hand, the time window should be constrained in length in order not to compromise the capability to reflect local variability of mining conditions and indicate anomalous variations in seismic activities in time. Based on reported field observations (McKavanagh and Enever, 1980; Styles *et al*., 1988), the time between the first notice of anomalous changes in microseismicity patterns and visible macroscopic failure or even rockbursts and outbursts spans over a wide range from 10 minutes, several hours, several days, to up to 17 days. As such, a ΔT of 14 days was used in this work, which covers microseismicity recorded over the last 10 working days. During holidays when coal extraction was halted for a longer time, ΔT was extended to cover the last 10 working days to prevent from the unfavourable impact of scarcity in recorded microseismicity. The forecasted probability of hazardous microseismic events was updated on a daily basis ($\Delta t = 1$ day) as a reference to timely evaluate the underground hazard potential.

Following the procedure described in Section 3, the probability of hazardous microseismicity and recommended upper limit of face advance were updated for each day from 14 days after the start of coal production until the completion of the panel.

5. RESULTS AND ANALYSIS

Fig. 11 presents the time-varying forecasted daily event number, and probability that large microseismicity, microseismicity close to the working face, and hazardous microseismicity occur on the day of forecasting for the panel K.-80/B. Recorded daily numbers of total microseismic events, large events, events close to the working face, and hazardous events are plotted respectively for validation.

The forecasted daily event counts from the statistical model show excellent agreement with recorded numbers of microseismicity, with large event counts being forecasted at high face advance rates, and no events being forecasted when the coal production ceases.

The probability of large microseismicity P_M was estimated according to Eqs. (3) and (7). The face advance rate on the day of forecasting affects the forecasted probability by tuning the forecasted event counts. When the coal production ceases at weekends or during holidays, the probability of large microseismicity is forecasted as 0 since the forecasted event count is 0. By comparison to b values analysis for weekly microseismicity around the same panel, the evolution of P_M and b values display distinctly opposite trends, which verifies that the decrease in the b value indicates an increase in the large event risk. The forecasted probability for microseismicity with an energy released greater than 10^5 J mostly stays at a high level (above 70%) on working days, and it can be seen that these events are quite common. By contrast, the forecasted probabilities for microseismicity at energy levels of 10^6 and 10^7 J show a tremendous decrease of several orders of magnitude, and such events are much less frequent. When the forecasted probability of microseismicity with $E > 10^7$ J around the K.-80/B panel reaches a peak of 6.5% and 12.9% on 19 and 20 April 2016, four such large microseismic events occurred around the same panel, two on each of those two days, respectively.
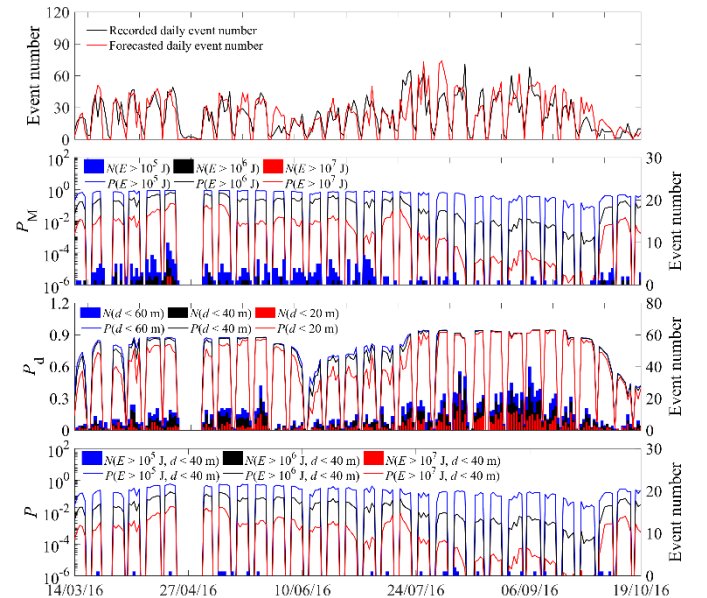

Fig. 11. Time-varying forecasted daily event number, and forecasted probability that at least a large microseismic event, a microseismic event close to the face-line, and a hazardous microseismic event occurs on the day of forecasting around panel K.-80/B.

The probability of microseismicity close to the working face was estimated according to Eqs. (3) and (8). This forecasted probability was also tuned by the face advance rate ratio. Considering the spatial distribution of microseismicity, microseismicity close to the working face are not as rare as large microseismicity. More microseismicity were recorded close to the working face when the statistical model estimates a higher probability of such events. As an example, the statistical model

estimates the probability that at least a microseismic event occurs close to the working face to be above 90% on working days between 25/07-23/09/2016 around K.-80/B panel, and the forecasted probabilities of microseismicity with $d < 60$ m, $d < 40$ m and $d < 20$ m have little differences. This is verified by recording a large number of microseismicity within 20 m distance to the K.-80/B face on those days.

The forecasted probability of hazardous microseismicity, which was estimated according to Eqs. (3) and (10), depends on all the three aforementioned forecasted results. In this figure, events within 40 m distance to the working face and having energy greater than 10^5, 10^6 and 10^7 J are considered as hazardous microseismicity. The forecasted time-varying probability of hazardous microseismicity closely follows the variation of that of large microseismicity (P_M), which means that the forecasting result is dominated by the impact of magnitude distribution of recorded microseismicity. By contrast, the forecasted probabilities of hazardous microseismicity are around one order of magnitude lower than those of large microseismicity with the same energy. As a result, only a few microseismicity with $E > 10^6$ J and $d < 40$ m and no microseismicity with $E > 10^7$ J and $d < 40$ m were recorded around the panel over the coal production period.

To optimise real-time control of longwall coal mining based on the probability forecasting, the recommended face advances for the panel K./-80B were calculated over the coal production period, using three probability limits (1%, 0.1% and 0.01%) for hazardous microseismicity ($E > 10^7$ J and $d < 40$ m), as shown in Fig. 12. Due to the large span of fracture sizes obeying the power law distribution, the back-calculated upper limits of daily face advance fluctuate tremendously at a linear scale from day to day. While a probability limit of 0.01% prohibits longwall mining over a considerable portion of the production period, probability limits of 0.1% and 1% allow higher face advance rates over the period of high hazard risks for the panel. The face advance rates back-calculated using site specific definition of hazardous microseismicity and probability thresholds can be used as a reference in adjusting the mine production schedule.
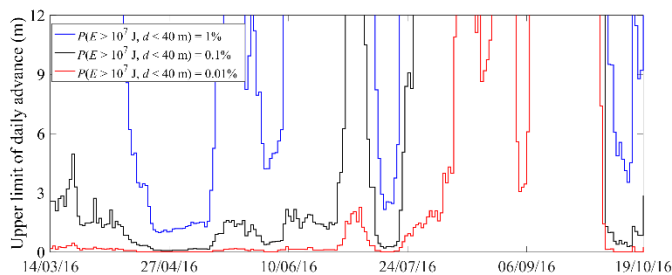

Fig. 12. Recommended upper limits of daily face advance given probability thresholds of hazardous events for panel K.-80/B.

6. CONCLUSIONS

Microseismic monitoring was carried out around eight longwall panels at Coal Mine Velenje over a 27-month coal production period. It was found that seismic energy magnitude and spatial distribution are dominated by those of underlying fractures, while microseismic event counts frequency is correlated with both local fracture abundance and mining intensity. On this basis, a statistical model to characterise temporal, magnitude and spatial characteristics of microseismicity was proposed, based on which hazardous microseismicity could be estimated and face advance regulated in real time. The statistical model was applied to forecast the potential of hazardous microseismicity and to further recommend upper limits of daily face advance for one longwall panel.

Results showed that the forecasted results agree well with microseismic monitoring results. In addition, results suggested that the energy magnitude distribution of microseismicity plays a dominant role in the potential of hazardous microseismicity. This statistical model using microseismic monitoring data has important implications in the evaluation of mining-induced hazards and optimal control of longwall face advance in burst-prone deep-level mining sites.

REFERENCES

Brady, B.T., 1977. Anomalous seismicity prior to rock bursts: Implications for earthquake prediction. *Stress Earth* 357–374.

Cao, W., J. Shi, G. Si, S. Durucan, A. Korre, 2018. Numerical modelling of microseismicity associated with longwall coal mining. *Int. J. Coal Geol.* 193, 30–45.

Fujii, Y., Y. Ishijima, G. Deguchi, 1997. Prediction of coal face rockbursts and microseismicity in deep longwall coal mining. *Int. J. Rock Mech. Min. Sci.* 34, 85–96.

Jeromel, G., M. Medved, J. Likar, 2010. An analysis of the geomechanical processes in coal mining using the velenje mining method. *Acta Geotech. Slov*. vol. 7, no. 1, pp.31-45.

Journel, A., C. Huijbregts, 1978. *Mining geostatistics*. Academic Press, London.

Kijko, A., C.W. Funk, A.V.Z. Brink, 1993. Identification of anomalous patterns in time-dependent mine seismicity, In *Proceedings of the 3rd International Symposium on Rockbursts and Seismicity in Mines*, 205–210.

Lasocki, S., 1993. Statistical short-term prediction in mining induced seismicity, In *Rockbursts and Seismicity in Mines*, 211–216.

Ma, T., C. Tang, S. Tang, L. Kuang, Q. Yu, D. Kong, X. Zhu, 2018. Rockburst mechanism and prediction based on microseismic monitoring. *Int. J. Rock Mech. Min. Sci.* 110, 177–188.

Marcak, H., 1993. The use of pattern recognition methods for prediction of the rockbursts, In *Proc. 3rd Int. Symp. on Rockbursts and Seismicity in Mines*, 223–226.

Markič, M., R.F. Sachsenhofer, 2010. *The Velenje lignite: its petrology and genesis*. Geological Survey of Slovenia, Ljubljana. ISBN 978-961-6498-20-3.

McKavanagh, B.M., J.R. Enever, 1980. Developing a microseismic outburst warning system, In *Proceedings of the Second Conference on Acoustic Emission/Microseismic Activity in Geologic Structures and Materials*, 211–225.

Melnikov, N.N., A.A. Kozyrev, V.I. Panin, 1996. Induced seismicity in large-scale mining in the kola peninsula and monitoring to reveal informative precursors. *Pure Appl. Geophys*. PAGEOPH 147, 263–276.

Richter, C.F., 1958. *Elementary Seismology*. WH. Freeman and Company, San Francisco.

Shearer, P.M., 1975. Introduction to Seismology, *Geophysical Journal of the Royal Astronomical Society*. doi:10.1111/j.1365-246X.1975.tb01612.x

Shen, B., A. King, H. Guo, 2008. Displacement, stress and seismicity in roadway roofs during mining-induced failure. *Int. J. Rock Mech. Min. Sci.* 45, 672–688.

Si, G., S. Durucan, S. Jamnikar, J. Lazar, K. Abraham, A. Korre, J.Q. Shi, S. Zavšek, G. Mutke, A. Lurka, 2015. Seismic monitoring and analysis of excessive gas emissions in heterogeneous coal seams. *Int. J. Coal Geol*. 149, 41–54.

Stewart, R.D., S.M. Spottiswoode, 1993. A technique for determining the seismic risk in deep-level mining, In *Proc. 3rd Int. Symp. on Rockbursts and Seismicity in Mines*, 123–128.

Styles, P., S.J. Emsley, T. Jowitt, 1988. Microseismic monitoring for the prediction of outbursts at Cynheidre Colliery, Dyfed, S. Wales. *Geol. Soc. London*, Eng. Geol. Spec. Publ. 5, 423–433.